




Cite this: *Lab Chip*, 2021, 21, 2383

A minimally invasive flexible electrode array for simultaneous recording of ECoG signals from multiple brain regions†

Ui-Jin Jeong,^{ab} Jungpyo Lee,^a Namsun Chou,^a Kanghwan Kim, ^a Hyogeun Shin,^{ac} Uikyue Chae,^{ab} Hyun-Yong Yu^b and Il-Joo Cho ^{*acde}

The minimal invasiveness of electrocorticography (ECoG) enabled its widespread use in clinical areas as well as in neuroscience research. However, most existing ECoG arrays require that the entire surface area of the brain that is to be recorded be exposed through a large craniotomy. We propose a device that overcomes this limitation, *i.e.*, a minimally invasive, polyimide-based flexible array of electrodes that can enable the recording of ECoG signals in multiple regions of the brain with minimal exposure of the surface of the brain. Magnetic force-assisted positioning of a flexible electrode array enables recording from distant brain regions with a small cranial window. Also, a biodegradable organic compound used for attaching a magnet on the electrodes allows simple retrieval of the magnet. We demonstrate with an *in vivo* chronic recording that an implanted ECoG electrode array can record ECoG signals from the visual cortex and the motor cortex during a rat's free behavior. Our results indicate that the proposed device induced minimal damage to the animal. We expect the proposed device to be utilized for experiments for large-scale brain circuit analyses as well as clinical applications for intra-operative monitoring of epileptic activity.

Received 16th February 2021,
Accepted 23rd April 2021

DOI: 10.1039/d1lc00117e

rsc.li/loc

Introduction

Multiple regions inside the human brain are organized functionally, and their activities are closely correlated with each other. Consequently, the investigation of the functional connectivity between more than two separate regions of the brain is very important in order to understand the mechanisms of brain functions and for the study of therapeutic methods for neurological disorders.^{1,2} Recently, electrocorticography (ECoG) has been used extensively for both clinical applications, such as intraoperative monitoring of epileptic activity, and the study of brain functions, such as functional cortical mapping.^{3–5} ECoG is a technique for measuring from the surface of the brain the collective neuronal signals that originate from the volume beneath the surface. Depending on the density of the signal-recording

electrodes on the array, ECoG may enable global mapping of the neuronal signals over a large area of the brain.^{6–8} The major advantage of ECoG over other electrophysiology techniques is that it does not penetrate the brain tissue. Therefore, the surgical procedure is less infectious and induces minimal inflammatory reactions. Due to this advantage, ECoG has been used in surgical procedures for the diagnosis of neuronal disorders in human subjects.^{3,7,9} For many intraoperative neuromonitoring and neuroscience applications, it is also necessary to record the local field potential (LFP) signals from multiple brain regions so that the foci of the neuronal disorder can be identified accurately and the correlations among the activities from the multiple brain regions can be studied.^{10,11}

To date, large-area, flexible-surface arrays of electrodes have been used to record the multi-region LFP from the surface of the brain.^{12,13} Flexible and biocompatible materials, such as polyimide, parylene, PDMS, and silk have been used to provide a conformal contact of the electrode arrays on the curved surface of the brain because their mechanical properties are similar to those of the brain.^{14–16} Even though the flexible array of electrodes can cover a large surface area and record the activities from multiple regions of the brain,^{17,18} these devices require a large cranial window for the placement of the electrodes.^{19,20} The formation of a large cranial window often leads to not only lowering the brain pressure and increasing the relative blood pressure but

^a Center for BioMicrosystems, Brain Science Institute, Korea Institute of Science and Technology (KIST), Seoul, Republic of Korea. E-mail: ijcho@kist.re.kr

^b School of Electrical Engineering, Korea University, Seoul, Republic of Korea

^c Division of Bio-Medical Science and Technology, KIST School, Korea University of Science and Technology (UST), Seoul, Republic of Korea

^d School of Electrical and Electronics Engineering, Yonsei University, Seoul, Republic of Korea

^e Yonsei-KIST Convergence Research Institute, Yonsei University, Seoul, Republic of Korea

† Electronic supplementary information (ESI) available. See DOI: 10.1039/d1lc00117e

also causing plasma to escape into the brain parenchyma and cause swelling because the brain is directly exposed to the air.²¹ Also, it has been studied that the craniotomy process using a dental drill, which must be performed to place the ECoG electrode in the cortex, causes proinflammatory, morphological, and behavioral damage.²² This process affects wound healing, as cortical damage increases as the craniotomy area increases. Therefore, it is highly required to minimize the exposed brain area to prevent any damage or inflammation on the brain.²³

To address the issue mentioned above, we developed a miniature, flexible electrode array composed of two recording parts that can be moved selectively with an external magnetic force for minimally invasive, multi-regional recording of ECoG signals. This flexible ECoG electrode array is fabricated with flexible material, *i.e.*, polyimide, using a precision micromachining process, and the small electrode array can be implanted through a small cranial window. A neodymium magnet, which is attached to the electrode array, enables accurate positioning of the electrodes within the epidural space with an external magnetic force applied from outside of the skull. A thin layer of a biodegradable polymer which is dissolved by the brain fluid after the positioning of the electrode not only holds the magnet and electrodes in place during the positioning step but also allows for simple retrieval of the magnet after the positioning step. The flexible electrode array can be attached firmly on the curved surface of the brain, enabling reliable recording of the ECoG signals at the target locations. Consequently, the device allows recording of ECoG signals in multiple regions of the brain using a minimally invasive method that is performed through a small cranial window. In order to demonstrate the capabilities of the proposed electrode array, we recorded ECoG signals from two distal brain regions in anesthetized rats. In addition, we successfully measured neural activities from both the visual cortex and the motor cortex regions in the animals. The light weight and the miniaturized size of the system allowed us to apply the system to the experimental animals. The results indicated that the proposed device can be used for a variety of animal experiments for studying the functional connectivity of the brain and that it could have other clinical uses as well.

Materials and methods

Fabrication of an ECoG electrode array

We used a 4-inch silicon wafer to fabricate a minimally invasive ECoG electrode array. First, a polyimide substrate layer was coated on the wafer at a thickness of 3.5 μm . Then, gold (Au) and titanium (Ti) adhesion layers were deposited at thicknesses of 300 nm and 20 nm, respectively, as signal lines and electrodes by e-beam evaporation, and they were patterned using a lift-off process. Next, microelectrodes (100 μm by 100 μm) were patterned with a photoresist. Then, a titanium (Ti) layer and a platinum (Pt) layer were deposited only on the microelectrodes at thicknesses of 20 nm and 150

nm, respectively, with sputtering, and this was followed by the lift-off process. After coating another polyimide layer for insulation, two polyimide layers were patterned using a plasma etching process in the shape of an electrode array. Then, the remaining photoresist was removed, and the device was detached from the wafer (Fig. S1†).

Mechanical stress simulation of the ECoG electrode array

We calculated the distribution of stress on the legs of the device during the electrode movement using COMSOL (COMSOL Multiphysics 5.3a; COMSOL, Inc.). For the simulation, the following values were utilized for the properties of polyimide: Young's modulus = 3.1×10^9 Pa, Poisson's ratio = 0.34, density = 1300 kg m^{-3} . We compared the legs in two different designs: straight and meandered. The dimensions of the parts of the legs are shown in Fig. S4A.† Both legs are 180 μm in width and 7 μm in height. The meandered leg has a portion with a serpentine structure at the first 2700 μm , and the length of each leg is 15 000 μm . We simulated the stress distribution on each leg with a lateral pressure of 0.05 N mm^{-2} applied at the end of the leg, where the electrode array is supposed to be located (Fig. S4B and C†).

Packaging of the ECoG electrode array

The fabricated electrode array was packaged according to the following procedure. The polyimide connecting part was taped up using Kapton tape to increase the thickness and mechanical strength to be able to fit into the zero insertion force (ZIF) connector (OMRON, Kyoto, Japan). This part was attached to a custom printed circuit board (PCB), and an Omnetics connector (Omnetics, Minneapolis, USA) was soldered on the other side of the PCB to provide electrical connections between the ECoG electrode array and the Intan recording system. Pt black was deposited on the Pt electrode through an electrodeposition method. After the fabricated ECoG electrode array was electrically connected to the PCB, the ECoG electrode (working electrode), Pt wire (counter electrode), and Ag/AgCl wire (reference electrode) were put in a Pt black plating solution. Thereafter, Pt black was deposited on the electrode with a voltage of -0.2 V applied across the working and the reference electrodes.

To move the flexible ECoG electrode array, a neodymium magnet with the dimensions of $1 \text{ mm} \times 1 \text{ mm}$ and thickness of 0.25 mm was attached to the recording part of the array (SM Magnetics, Pelham, USA). For the attachment process, we used sucrose gel, which is a biocompatible and biodegradable organic compound (Sucrose, Sigma, Darmstadt, Germany). The concentration of sucrose in the gel determined the dissolution time. While a higher sucrose concentration results in a longer dissolution time, we optimized the concentration of sucrose gel as 70%, which was the maximum solubility of sucrose in deionized water. We attached the recording part to the magnet using 70% sucrose gel as an adhesive *via* the following process: first, we

placed the device on a slide glass and dispensed 0.2 μL sucrose gel on the device to form a droplet. Then, a neodymium magnet was placed in contact with the slide glass on the opposite side. Next, we attached the device magnet to the sucrose gel. Then, we hardened the sucrose gel in an oven at 80 $^{\circ}\text{C}$ for 20 minutes after which we removed the magnet on the bottom side of the slide glass. Finally, we released the device from the slide glass (Fig. S3A†). The magnetic attraction between the two magnets allowed us to repeatedly apply an appropriate amount of force so that we can reliably control the thickness of the sucrose gel. The thickness of the sucrose gel produced was approximately 20 μm (Fig. S3B and C†).

Electrochemical impedance

After the fabrication and packaging processes, we performed electrochemical impedance spectroscopy (EIS) on the electrodes over the frequency range of 1 Hz to 10 kHz using a commercial impedance analysis system (Autolab, Metrohm Autolab, The Netherlands). To measure the EIS, we immersed

the working electrode (our electrode) and the reference electrode (the Ag/AgCl electrode) in an electrolyte (1 \times phosphate-buffered saline (PBS) solution).

Positioning of the electrode

The whole surgical process was performed on a stereotaxic frame. After positioning the anesthetized rat on a stereotaxic frame (David Kopf Instruments, USA), the skin over the part of the skull over the desired hemisphere of the brain was removed, and we marked target positions on the exposed skull. The precise location of the target region was calculated based on the stereotaxic coordinates from Paxinos and Franklin's atlas. Next, we drilled a 1.5 mm diameter hole on the skull. We inserted one recording part and guided it with a magnet from outside the skull (Fig. 1B). We confirmed the movement of the device by watching the movement of the leg being pulled into the skull along the direction of the movement. It was also possible to check the moving procedure of the electrode array in real time under a

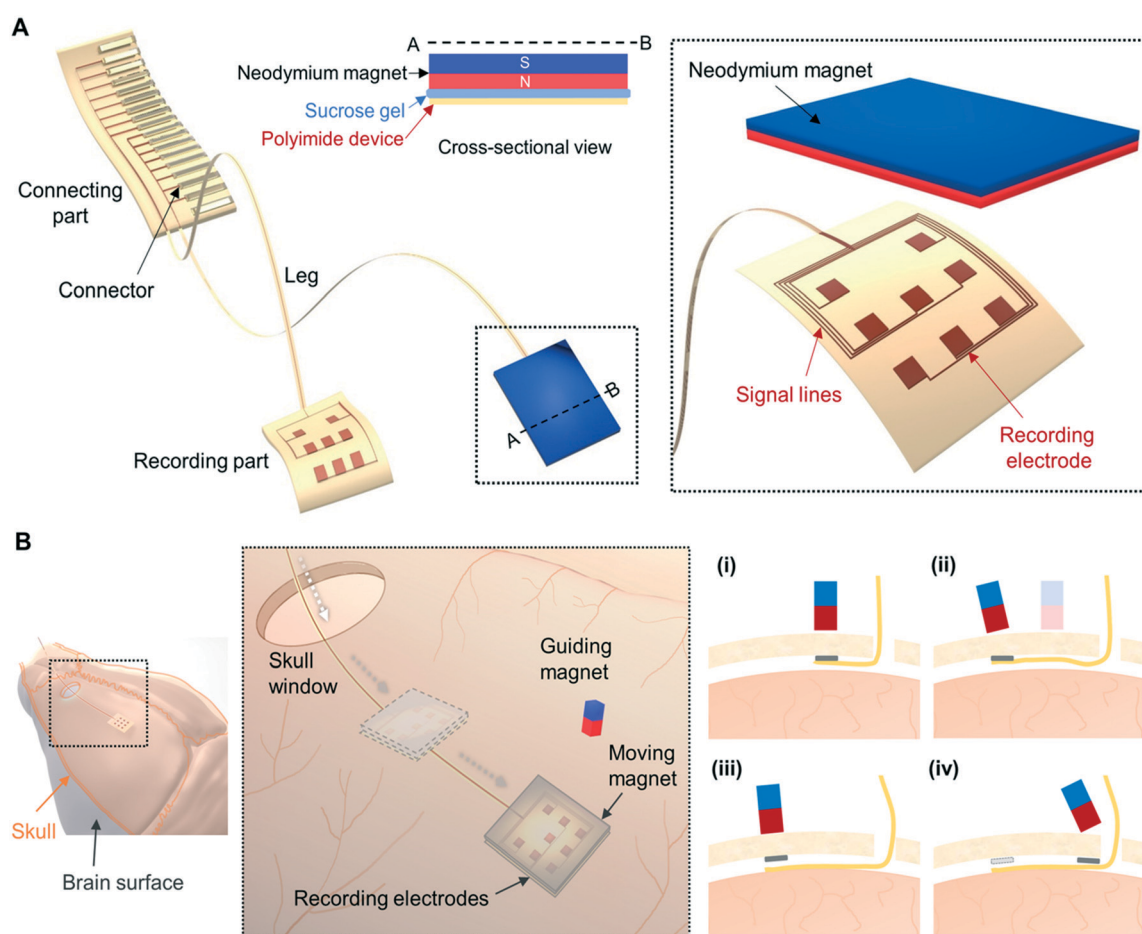


Fig. 1 Structure of the flexible ECoG electrode array. (A) Schematic diagram of the proposed flexible ECoG electrode array and cross-sectional view of the recording part (thickness; neodymium magnet, 250 μm , sucrose gel, 20 μm , polyimide device, 7 μm). (B) Conceptual diagram of the device positioning process through a small skull window on the rat's brain: (i and ii) electrode array implanted through a small cranial window and moved to the target region, (iii) sucrose is melting and the device is attached on the brain, (iv) device magnet is retrieved outside of the brain.

microscope as the outline of the electrode was visible under the skull using a focused illumination for the microscope.

In vivo acute recording

All of the procedures that involved the use of rats were approved by the Korea Institute of Science and Technology (KIST) in Seoul, Korea, and the procedures were conducted following the ethical standards stated in the Animal Care and Use Guidelines of the KIST. The ECoG electrode array was tested using adult male Sprague Dawley rats (SD rats, 8 weeks, 250–270 g). The rats were anesthetized with urethane (1.5 g kg^{-1} , intraperitoneal injection) in the acute recording experiment. We made a hole on the motor cortex based on Paxinos and Franklin's atlas (coordinates: AP = -1.0 ± 0.5 , ML = $\pm 1.0 \pm 0.5$ mm relative to bregma). Next, one recording part was moved to the visual cortex (coordinates: AP = $+1.0$ and ML = $\pm 3.5 \pm 1.0$ mm relative to lambda) using external magnetic force, and the other recording part was placed on the motor cortex region through the hole. After the recording part was attached to the surface of the brain and the sucrose gel was degraded with cerebrospinal fluid (CSF), we collected the moving magnet. ECoG signals were recorded in the anesthetized state using an Intan recording system (Intan RHD 2132 system, Intan Technologies, Los Angeles, California). The raw signals were filtered and digitized through the Intan software (25 kS s^{-1} per channel, 0.1 Hz to 6 kHz band-pass filter for ECoG, 60 Hz notch filter).

Chronic recording of multi-regional ECoG signal

We implanted the electrode array on the multi-region cortex area in the rat's brain using a minimally invasive method. The experiment was conducted on adult male SD rats (8 weeks, 250 g to 270 g). The rats were anesthetized initially with 3.5% isoflurane (Terrell Solution, Piramal Healthcare) combined with O_2 and N_2O and maintained the anesthesia state with 2% isoflurane. The surgical procedure and device positioning process are described in the Positioning of the electrode sub-section. After positioning the electrodes in two target areas, *i.e.*, visual cortex and motor cortex, we attached the PCB and device to the head of the animal and encapsulated the PCB. We used screws and dental cement to fix the device on the head. First, we inserted four screws into the skull and used them as supports for dental cement application. Then, we placed the PCB on the skull, applied dental cement in the space between the fixed screws and the PCB, and waited until the cement cures for 40 minutes.

Two weeks after electrode insertion, two types of experiments were performed in awake rats to estimate specific ECoG signals in the visual and motor cortex. Animals with ECoG electrodes inserted were set free to move freely within the behavioral test box which measures $50 \times 50 \times 40 \text{ cm}$ ($W \times L \times H$). First, we measured the ECoG signal from a behaving animal with visual stimulation. Visual stimulation was applied using a commercial flashlight

inside a dark action box. The duration of light was 50 ms, and the frequency was 12.5 Hz. The experiments were performed in the dark, and the intensity of the flashlight was 25 lm. Baseline ECoG signals were measured for 30 minutes before stimulation, and visual stimulation experiments were conducted for 30 minutes. In the visually stimulated condition, the rat was in the behavior box, and we recorded the ECoG signal using the Intan recording system. Second, we measured the ECoG signal of freely moving rats and classified the pattern of the ECoG signal by behavior. We let the rat move freely in the behavior box without any external stimulus. We have defined five detailed actions as follows:

- Climbing: a rat tried to climb up the wall of the chamber. The forelegs were on the wall, and the hind legs were on the bottom.
- Walking: a rat was walking freely in the chamber.
- Standing: a rat stood with its forelegs in the air and supported itself only with its hind legs.
- Sniffing: a rat sniffed and smelled with its nose through the air, moving only the whiskers.
- Stepping: a rat was sniffing and stepping its forelegs repeatedly but did not change its location.

These five subgroup activities were divided into two main groups depending on the location of the rats. Climbing, walking, and standing are classified as moving behaviors because the position of the rat dynamically changes according to the behavior. Also, the actions of smelling and stepping were classified as resting actions because the rats kept their position fixed. ECoG signals from the rats were recorded using the Intan recording system. The raw signals from all chronic recordings were filtered and digitized through the Intan software (25 kS s^{-1} per channel, 0.1 Hz to 6 kHz band-pass filter, 60 Hz notch filter).

Histology and immune response test

To evaluate any damage to the cortex, we conducted a histological analysis of the brain. The rats were perfused transcardially with cold physiological saline followed by 4% paraformaldehyde in 0.1 M PBS. After overnight postfixation in the same fixative, the brains of the rats were immersed in 30% sucrose in 0.1 M PBS for two days. Coronal sections were cut into 30 μm thickness using a sliding microtome. The 30 μm -thick brain slices were washed in 0.1 M PBS and blocked in a blocking solution containing 0.1% [v/v] Triton X-100 and 3% [w/v] bovine serum albumin (BSA) in 0.1 M PBS for 2 hours at room temperature. For immunofluorescence staining, each section was stained with primary antibody (chicken anti-GFAP, 1:500, EMD Millipore, ab55411; mouse anti-Tuj1, 1:500, Sigma, T8578; rabbit anti-Iba1, 1:500, Fujifilm, 019-19741). After washing three times in 0.1 M PBS for 30 min, the primary antibody-conjugated brain slices were incubated with secondary antibodies (mouse anti-goat conjugated Alexa Fluor 488, 1:500, Invitrogen, ab11001; rabbit anti-goat conjugated Alexa Fluor

594, 1:500, Invitrogen, a11011; chicken anti-goat conjugated Alexa Fluor 647, 1:500, Abcam, ab150171) in 0.1 M PBS containing 3% [w/v] BSA for 2 hours at room temperature. After washing five times in 0.1 M PBS for 30 min, the brain slices were incubated with 4',6-diamidino-2-phenylindole (DAPI; 1:1000, Invitrogen, 1306) in 0.1 M PBS containing 3% [w/v] BSA for 30 min at room temperature. After washing, the sections were mounted on cover slides with a mounting medium. Sections were observed in a fluorescence microscope image.

Analysis of ECoG signal

All analyses were performed using MATLAB (MathWorks, USA) and GraphPad Prism (GraphPad Software Inc., USA). We analyzed the frequency components of the recorded signals from each region using spectrograms obtained *via* fast Fourier transform. We also analyzed spontaneous ripple oscillations by looking at the 100–250 Hz frequency band. Finally, the recorded signals were band-pass filtered with appropriate filters to extract theta, alpha, beta, and gamma waves.

Results and discussion

Design of the minimally invasive, flexible ECoG electrode array

The proposed electrode array was designed as a flexible and thin structure so that it could be moved freely inside the epidural space. The ECoG electrode array consists of two recording parts, legs, and a connecting part, which allow each of the recording parts to be positioned independently in the target area for multiple-regional recording (Fig. 1A).

The most important consideration in the design of our ECoG electrode array is to have a recording electrode array for large spatial coverage and long flexible legs that provide the strength to move the electrodes freely. Also, the substrate in which the electrode array is located is flexible so that it can be attached conformally to the curved surface of the brain.

The electrode array consists of 16 channels and the recording parts have 8 electrodes in each for multiple-area measurement. We designed the size of each electrode to be 100 μm by 100 μm because this size has been used extensively for measuring ECoG signals.¹² The size of the

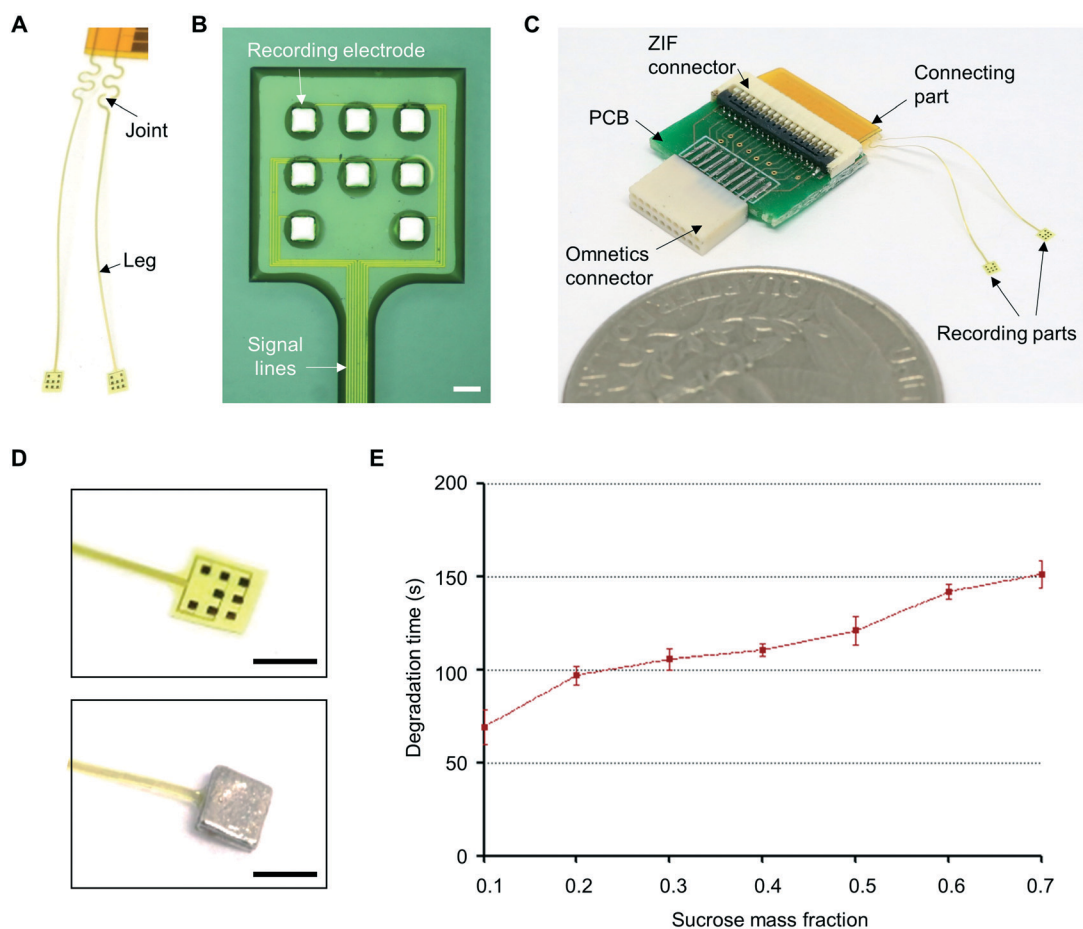


Fig. 2 Image of fabricated ECoG electrode array. (A) Image of the flexible recording parts and legs. (B) Microscopic image of the ECoG electrode array with eight 100 μm \times 100 μm -sized electrodes (scale bar, 100 μm). (C) Optical image of the packaged device. (D) Image of the packaged electrode attached with a moving magnet using sucrose (top: electrode array; bottom: electrode with a moving magnet) (scale bar, 1 mm). (E) Degradation time of sucrose gel used for packaging per concentration (average of 5 samples each concentration).

recording part was 1 mm by 1 mm, which is smaller than that of previous ECoG arrays, but this size was sufficient for the rat cortex microcircuit regions, and it was large enough to have a permanent magnet attached. Also, the leg was designed for connecting the electrodes, and the connecting part was 200 μm wide and 15 mm long to ensure the free movement of the recording parts. The thickness of the leg was only 7 μm , which results in a highly flexible and bendable structure with a small curvature radius based on previous research.^{15,24} It gently connects the connecting part with electrodes and minimizes the possibility of damage to the surface of the brain during movement. Most notably, we designed joints with a curved structure in the legs to allow freedom of movement below the skull and relieve stress. Specifically, the joints with a curved structure distribute stress evenly to the meandering parts and thus alleviate breaking caused by stress (Fig. 2A and S4†). The connector, which included 18 pads, was designed for making connections between electrodes and the external amplifier, and the sizes of the pads were designed to be compatible with commercial connectors.

The purpose of our design was to allow the electrodes to move freely into the target region through the shallow epidural space inside the skull. Our electrode array was a thin, flexible structure, which made it possible to pass it through the shallow space so we could locate the electrode on the target area and measure the neural activities from multiple regions through a minimal surgical opening (Fig. 1B).

Fabrication and packaging of the ECoG electrode array

We fabricated the flexible electrode array with small electrodes based on microfabrication technology that enabled small, thin mechanical structures with precise control of their dimensions (Fig. S1†). We fabricated the array with a thin polyimide layer, which is being used as substrates and insulation layers in flexible ECoG arrays with its biocompatible properties, in conjunction with Au and Pt electrodes. This thin (7 μm thick) flexible structure ensured the conformal contact of the electrode array with the curved surface of the brain (Fig. 2B). To insulate the signal lines, their tops and bottoms were encapsulated with polyimide layers that were 3.5 μm thick, and the Pt electrodes were exposed by patterning the top polyimide layer.

Next, we packaged the electrode array for the *in vivo* experiments (Fig. 2C). We connected the ECoG electrode on a custom printed circuit board (PCB) through an 18-pin zero insertion force (ZIF) connector (OMRON, Kyoto, Japan), which is easily plugged without soldering, and the other side of the PCB was connected to a recording system using an Omnetics connector (Omnetics, Minneapolis, USA). The weight of this packaged device was only 0.33 g, which was light enough to apply to a rat without significant restriction of the rat's behavior.

Then, we bonded a 0.25 mm-thick neodymium magnet (1 mm \times 1 mm), which is the strongest type of permanent

magnet that is available commercially, on the recording part so that we could move the recording part with an external magnetic force (Fig. 2D).²⁵ After locating the recording part, we also retrieved the magnet with external magnetic force. Thus, we bonded the magnet using biodegradable material, which eventually would be dissolved by the brain fluid. We selected sucrose gel, which is used extensively due to its biodegradable and biocompatible properties.²⁶ During the insertion process, the sucrose gel should sustain the bonding and be dissolved after locating the recording part. Thus, we optimized the degradation time of the sucrose gel by varying the concentration because the degradation time of sucrose increases as its concentration increases.²⁷ We observed that the higher sucrose concentration induced a longer degradation time, and we optimized the concentration as the maximum solubility of sucrose gel in deionized water, which is about 70% (Fig. 2E). The thickness of the sucrose gel was about 20 μm , which did not induce a significant increase in the total thickness. The solidified sucrose gel was used to attach the electrode array to the magnet, and the degradation time was found to be about 2 minutes at body temperature (37 $^{\circ}\text{C}$), which was enough time to locate the electrode in the target region. The magnet was collected by separating it from the electrodes using the water-soluble property after locating the recording part in a target position.

For recording the ECoG signals *in vivo*, it is important to reduce the impedance of the electrodes, so we electroplated black Pt on the deposited Pt electrodes. The roughness of the electroplated Pt enhanced the surface roughness and improved the impedance of the electrodes (Fig. S2†). The average impedance of the electrodes decreased from 0.1 M Ω to 0.005 M Ω at 1 kHz after the electroplating of black Pt, which was sufficiently low to record ECoG signals on the surface of the brain.^{17,18}

Insertion and location of the ECoG electrode array

Prior to the *in vivo* experiments, we set the procedures for inserting the electrode array through a small hole and positioning the electrode on the target regions of the brain with external magnetic force. Fig. 3A illustrates the positioning process of this electrode as a cross-sectional image. We used a neodymium magnet for applying an external magnetic force to the magnet attached on the recording part. The diameter of the external cylindrical magnet was 1 mm, and its height was 40 mm. The calculated surface magnetic force between the guiding magnet and the moving magnet was 0.02 N, which was sufficient for operating through a skull that was 1 mm thick.^{28–31}

The total thickness of the packaged electrode was 280 μm , so it could be moved freely through the 300 μm epidural space.³² The thickness of the packaged recording part was thinner than the height of the epidural space.³³ We controlled the position of the recording part under the skull by moving the external magnet on the skull (Video S1†). With this process, the electrode, with its thin, conformal, and

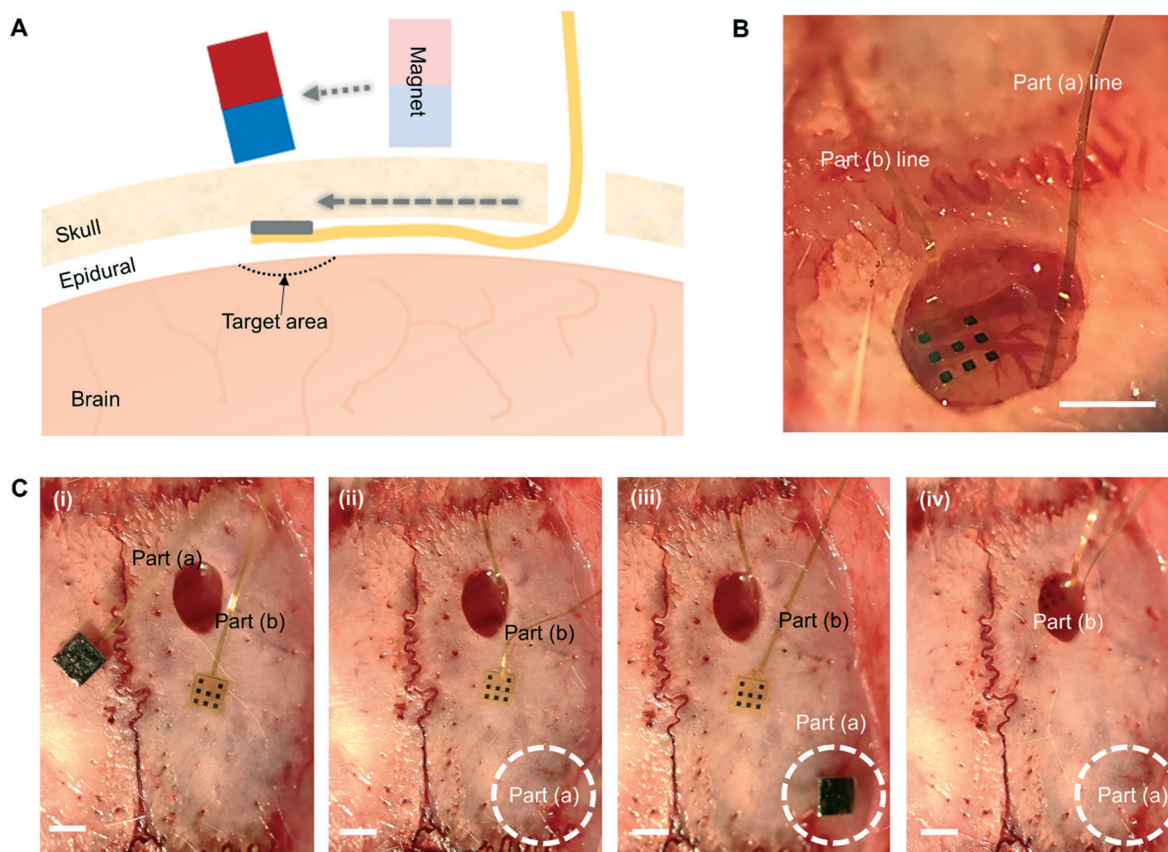


Fig. 3 Positioning procedure of the flexible ECoG electrode array. (A) Cross section of the device guiding procedures. (B) Microscopic image of the recording scene: part (a), moved device; part (b), positioned device near the hole; scale bar: 1 mm. (C) Procedures for positioning the recording electrode on the target region: (i) each one of the parts is not positioned, (ii) device part (a) is moved to the visual cortex region, (iii) moving magnet of device part (a) is taken away to the outside of the skull, (iv) device part (b) is positioned near the hole; scale bar: 1 mm.

flexible structure, was positioned successfully on the target region of the brain (Fig. 3B). We also investigated the possible damage induced by the movement of the magnet through histological data (Fig. S5†). When we compared the population of neurons between the surface of the brain where the electrode moved and the surface of the intact brain, there was no significant difference, and we could confirm that there was little damage to neurons (Fig. S6†). In addition, an observation of the inner surface of the skull revealed little physical damage on the skull (Fig. S5C†). Accordingly, we conclude that the movement of the electrode with a magnet does not induce significant damage on both the brain surface and the inner surface of the skull. Furthermore, the proposed structure is composed of only biocompatible materials such as polyimide, gold, and platinum, which ensures the biocompatibility of the ECoG electrode array.

Initially, an electrode-sized target hole was exposed with minimal surgery (Fig. 3C, i). One part of the electrode, combined with a moving magnet, was moved to the target area by the magnetic force between the external magnet and the moving magnet (Fig. 3C, ii). We were able to observe the magnet moving under the thin skull, which enabled us to position the electrode array at the target region of the brain. After the electrode array was positioned properly, we waited

10 minutes for the stabilization and the adhesion of the electrode array on the cortex of the brain with surface tension due to the thin and flexible structure. During this time, the moving magnet and electrode array were detached from each other when the body fluid dissolved the sucrose, and we could successfully retrieve the moving magnet and move it outside of the skull (Fig. 3C, iii and Video S2†). During the retrieval of the magnet, we could confirm the staying of the electrode array in place because the leg that came out of the hole did not move. The thin electrode structure composed of polyimide ensured the conformal contact on the curved surface of the brain. Then, we located the other electrode on another region of the brain and recorded ECoG signals from multiple regions simultaneously (Fig. 3C, iv).

Multi-regional acute ECoG recording

First, we confirmed the capability of the electrode array that was fabricated for the simultaneous recording of ECoG signals from two distant regions of the brain of an anesthetized rat. We recorded signals from the motor cortex and the visual cortex, which are located far from each other (approximately 4 mm apart) and are well known for generating distinctive signals.^{11,34}

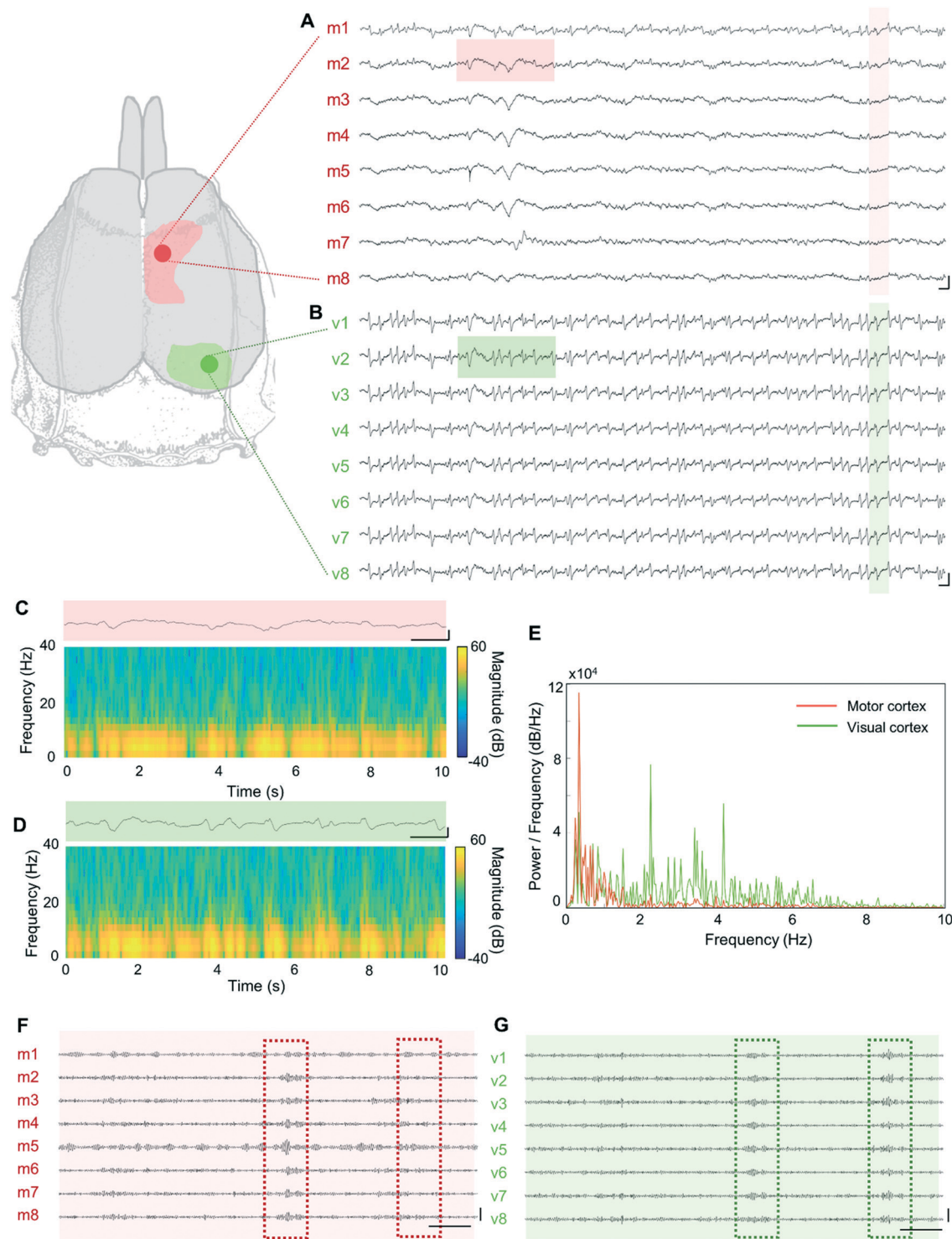


Fig. 4 Simultaneous acute ECoG recording from two different regions. Raw ECoG signals recorded from the motor cortex (A) and the visual cortex (B) (scale bars: 1000 μ V, vertical; 1 s, horizontal). (C) Representative frequency spectrogram of LFP from recording channel m2 of the motor cortex (scale bars: 1000 μ V, vertical; 1 s, horizontal). (D) Representative frequency spectrogram of LFP from recording channel v2 of the visual cortex (scale bars: 1000 μ V, vertical; 1 s, horizontal). (E) ECoG power spectrum densities on each area (green, visual cortex; red, motor cortex). (F) Ripple signal of band-pass filtered motor cortex signal (scale bars: 50 μ V, vertical; 200 ms, horizontal). (G) Ripple signal of band-pass filtered visual cortex signal (scale bars: 50 μ V, vertical; 200 ms, horizontal).

The waveforms of the ECoG signals recorded from all of the eight electrodes in the same area were similar,

irrespective of their micro distances. However, the patterns of the waveforms recorded from the different regions of the

brain were significantly different (Fig. 4A and B). The characteristic high-amplitude synchronous oscillations, which typically are observed in a brain under urethane anesthesia, were more clearly visible in the signals from the visual cortex.³⁵ Also, we observed a clear difference in the frequency spectrum in each cortex (Fig. 4C and D). The clear

difference between the signals recorded from the different regions also was reflected in the power spectrum density (PSD) plots of the signals, especially in the low-frequency band (0–10 Hz) (Fig. 4E).³⁶

We could measure the slightly different ripple signals by the location of each electrode in the same region as

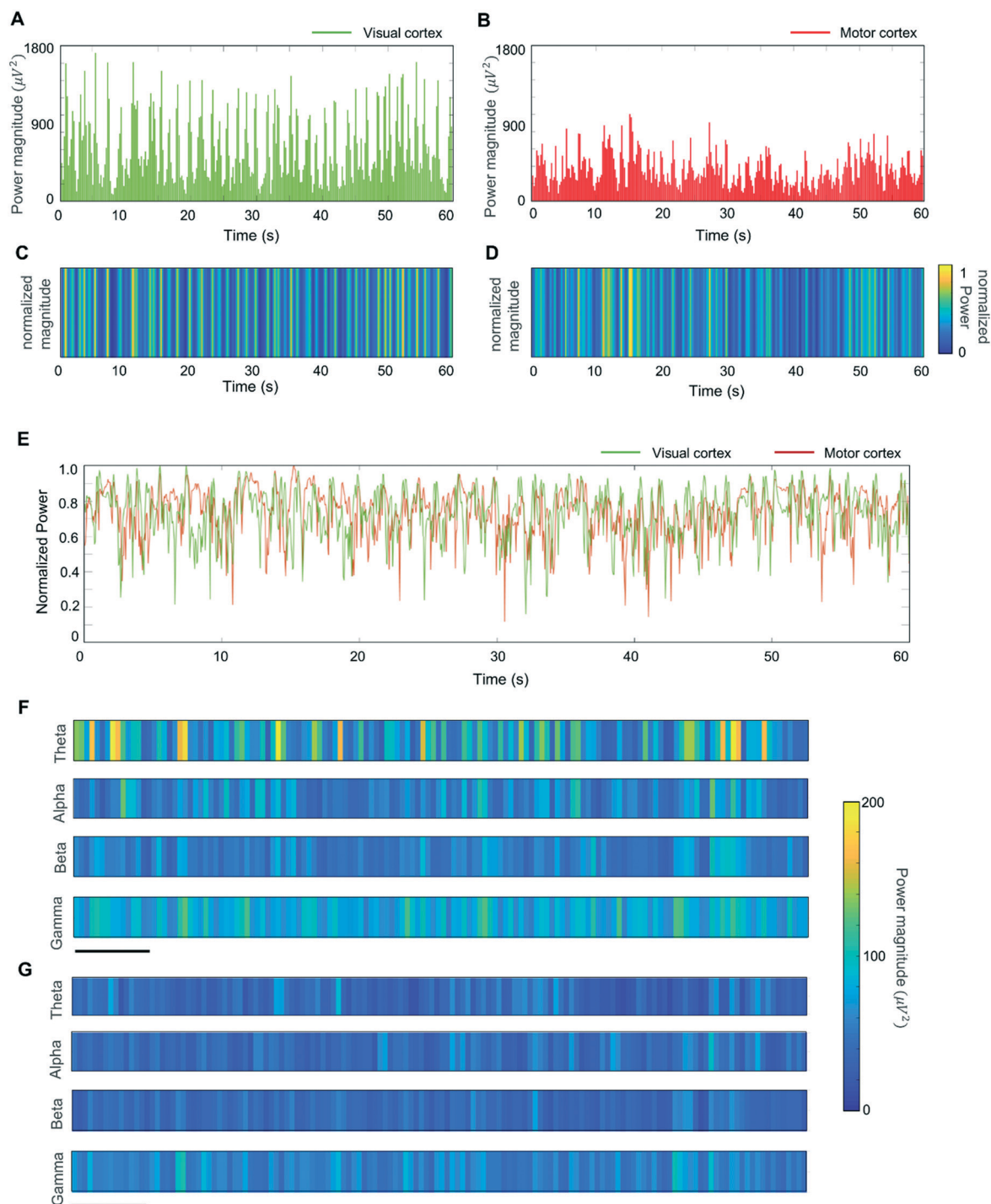


Fig. 5 Analysis of the ECoG signals of multi-regional acute recording. Integrated delta frequency of the visual cortex (A) and the motor cortex (B) in unit time interval. Normalized magnitude of delta frequency power of the signal recorded from the visual cortex (C) and the motor cortex (D). (E) Magnitude of mean normalized power of signals from the visual cortex and motor cortex, respectively. Various brain wave analyses in unit time interval of signals from the visual cortex (F) and motor cortex (G) (scale bar: 10 s; theta, 4–8 Hz; alpha, 8–13 Hz; beta, 16–30 Hz; gamma, 32–100 Hz).

well as region difference (Fig. 4F and G).^{37–39} Since these hippocampal ripples are delivered to a widespread activation pattern across almost every area of the cortex,

we could confirm that our electrodes successfully measured the ECoG signal which contained these ripples.⁴⁰

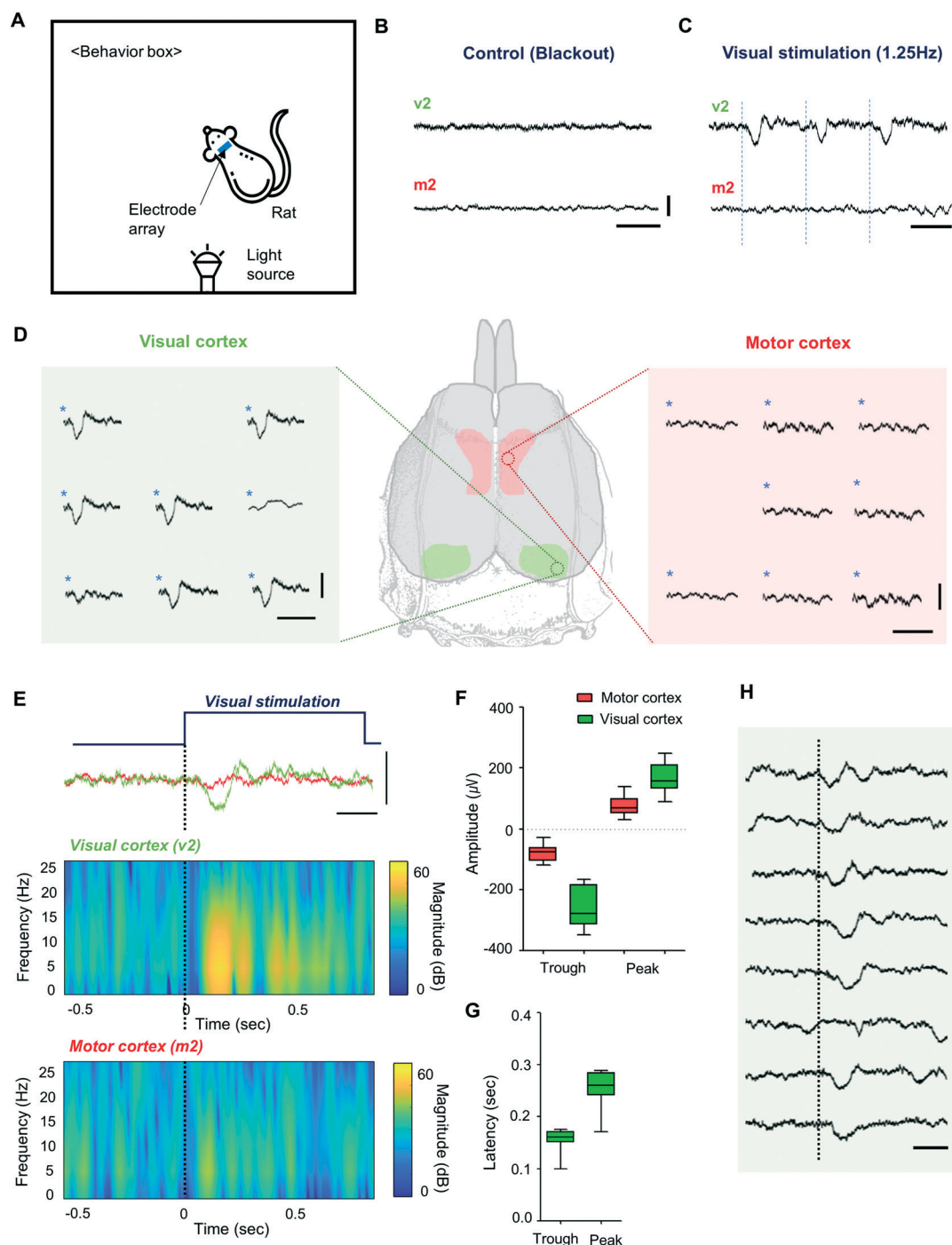


Fig. 6 Chronic multi-regional ECoG signal in visually stimulated condition. (A) Schematic diagram of the experimental setting for light stimulation in the behavior box. (B) ECoG signal of representative channel in dark condition, control experiment (top: visual cortex, v2; bottom: motor cortex, m2), (scale bars: 500 μ V, vertical; 500 ms, horizontal). (C) ECoG signal in the visual stimulation condition of the representative channel (top: visual cortex, v2; bottom: motor cortex, m2) (scale bars: 500 μ V, vertical; 500 ms, horizontal). (D) Signal comparison of 8 electrodes in response to light stimulation (scale bars: 500 μ V, vertical; 500 ms, horizontal; *, stimulation time). (E) Frequency spectrogram of stimulated condition (top: visual cortex, v2; bottom: motor cortex, m2) (scale bars: 500 μ V, vertical; 200 ms, horizontal). (F) Comparison of the amplitude of the trough and the peak in each area. (G) Latency time of trough and peak from stimulation time on the visual cortex. (H) Delay of visually evoked signals in the visual cortex (scale bars: 500 μ V, vertical; 200 ms, horizontal).

Next, we measured and compared the delta frequency band corresponding to the low-frequency range (0.1–4 Hz), and it is one of the most representative brain waves that can be measured in a deep sleep state, so it was measured dominantly in the cortex of the anesthetized rat.⁴¹ Consequently, we compared the magnitude of the delta wave frequency oscillation of the visual cortex and the motor cortex (Fig. 5A and B). Then, we normalized the magnitude of the power and observed the delta band signal difference of each area with the peak time of each area (Fig. 5C and D). This tendency can also be expressed with mean normalized power (Fig. 5E).⁴² We also compared the magnitude of the overall brain waves, *i.e.*, the theta wave (4–8 Hz), the alpha wave (8–13 Hz), the beta wave (16–30 Hz), and the gamma wave (>30 Hz). These spectrum results show the tendency of the total power magnitude (Fig. 5F and G).

Notably, we confirmed that the brain waves recorded in the two areas were different, which means we can record the signal in each area independently. Therefore, our flexible ECoG electrode array provided the capability of measuring signals in multiple areas.

Chronic multi-regional ECoG recording

We investigated the multi-regional activating ECoG signal with the minimally invasive flexible ECoG electrode array in freely behaving rats. We implanted the electrode array and located the electrodes on the primary motor cortex (M1) and the primary visual cortex (V1) according to Paxinos and Watson's atlas.³⁴ Then, we fixed the implanted electrode array on the animal's head. After the animal recovered, we recorded neural signals from the electrodes in the freely behaving condition for two weeks to confirm that the device could stably record ECoG for an extended period of time. The signals were recorded inside a chamber, and the animal was free to move around with the light weight and small size of the implanted device (Fig. 6A). This paper provides the results of behavioral experiments that were conducted to show the specific ECoG signals of the visual cortex and the motor cortex.

We found that the electrode array could record the neural activity that occurred in response to external stimulation. To confirm this, we designed a visually stimulated condition and recorded the resulting ECoG signal. We provided optical stimuli to the animal using a flashlight inside the blackout chamber. ECoG signals from the visual cortex and the motor cortex were recorded during periodic optical stimulation ($f = 12.5$ Hz) that was provided with a flashlight (Fig. S7†). While there was no characteristic difference in the signals recorded from the two regions in the absence of optical stimulus, the recorded signals from the visual cortex showed activities highly synchronous to the optical stimulation when periodic optical stimuli were provided (Fig. 6B and C).^{43,44} Interestingly, the recordings from different electrodes from the same region showed slightly different signals (Fig. 6D).⁷

In the light-stimulated condition, the evoked signal of the visual cortex indicated more synchronized neural activity from activation of the large population of neurons.^{45,46} We compared the properties of the signals of each area, and Fig. 6E shows that the V1 in the stimulated condition resulted in a more activated frequency spectrogram. The amplitudes of the troughs and peaks of the signals also provided information about these differences (Fig. 6F). There were the visual pathways that deliver stimulation accepted from the retina to the visual cortex, which is located in the occipital lobe. The latency in response to visual stimulation is known to be 100 to 200 milliseconds in rats that are awake.⁴⁵ We plotted these delivery latencies from stimulation and confirmed that the values were similar to previous results (Fig. 6G and H).^{7,47}

Also, we detected that the voluntary movements of the animals induced brain activity. To confirm this, we measured the change in the ECoG signal with the movements of the rats. Interestingly, the ECoG signals based on moving behavior allowed us to observe the correlation between the behaviors and specific brain waves of the LFP signal in the relevant areas. To study these behavioral signals, we let a rat with the chronically implanted ECoG electrode behave freely in the chamber described above. The experiments were conducted in an empty behavior box with only weak lighting for fewer stimulation conditions. The rats were not disturbed or stimulated, so their actions occurred freely and voluntarily. We found that the rats showed a variety of behaviors, *e.g.*, climbing, walking, standing, sniffing, and stepping. We classified these five subgroup activities into two main groups based on the moving of the rat's location. If the rat stayed in one location, we classified it as resting behavior. Behavior that involved moving and changing locations was classified as moving behavior.

During the freely-moving activity in the behavior chamber, motor cortical ECoG signals were recorded and found to have significant fluctuations compared to the visual cortex (Fig. 7A and B). In particular, it was apparent that the ECoG signal during the moving status was much more active than it was during the resting status (Fig. 7C and D). At this time, the ECoG signal waveforms of eight electrodes recorded from the same area showed distinctly different patterns among the rats in voluntary moving conditions (Fig. S8†). Also, we observed the correlations between the theta wave oscillations and the moving status on the motor cortex. Theta oscillations of the hippocampus are generally known for their relation to the moving behavior and locomotion activity of rats.⁴⁸ The results of the measurements of the electrical activity of the motor cortex during free-moving behavior proved the connection between voluntary movement and the theta wave oscillation spectrum (Fig. 7B and S9†). The LFP recorded during moving showed a more significant increase in the output of the delta band (~2 Hz) and the theta band (4–8 Hz) compared to the stationary resting states, indicating consistent results compared to previous studies (Fig. 7E and F).⁴⁹

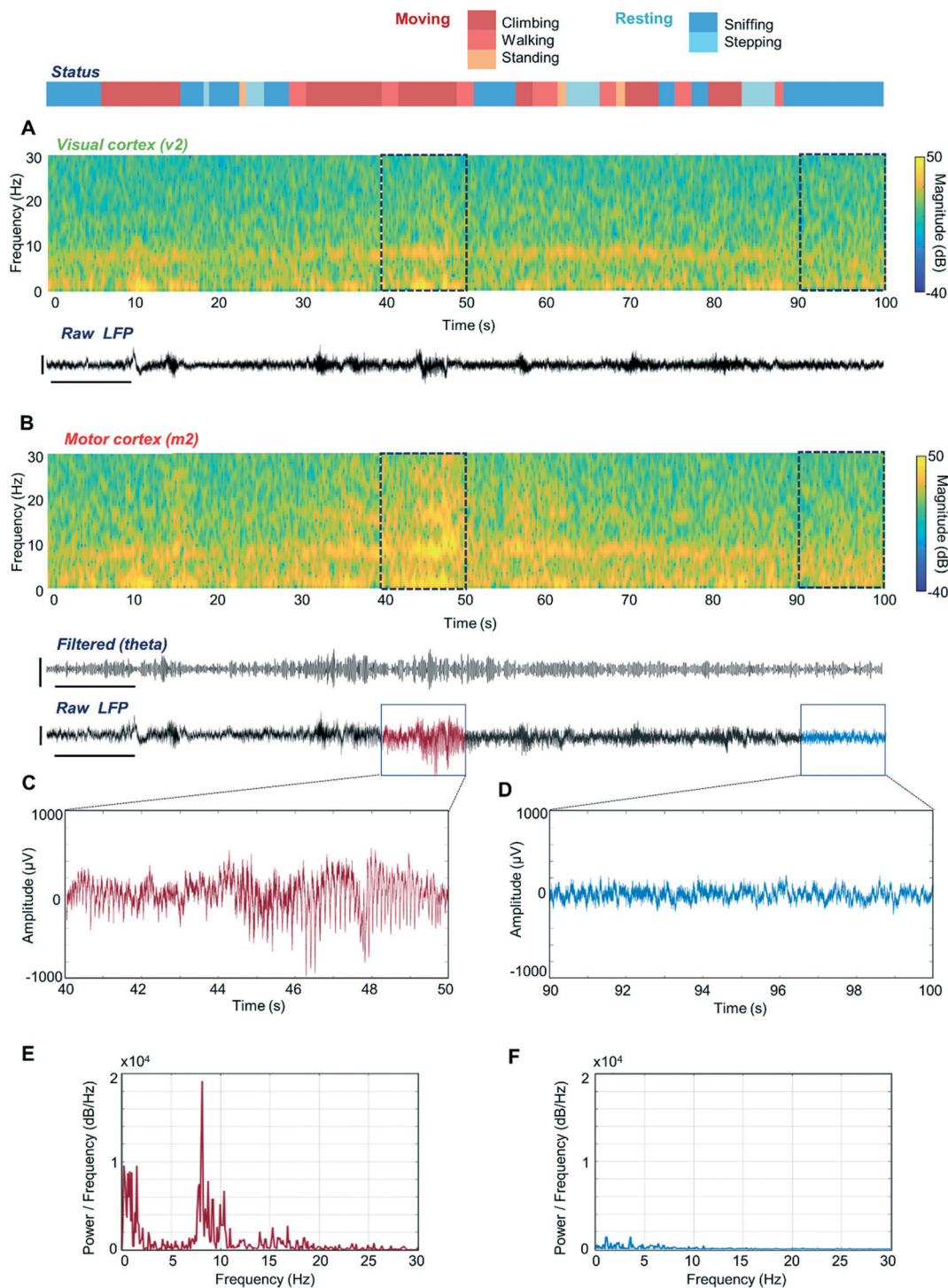


Fig. 7 Activated ECoG signal of freely behaving rats. (Top) Status of rat behaviors over time. (A) Representative frequency spectrum of ECoG signal recorded from the visual cortex and raw LFP in behaving condition of channel v2 (scale bars: 500 μ V, vertical; 10 s, horizontal). (B) Representative frequency spectrum of ECoG signal recorded from the motor cortex in behaving condition of channel m2 (top), theta wave filtered data (middle; scale bars: 400 μ V, vertical; 10 s, horizontal), raw LFP signal (bottom; scale bars: 500 μ V, vertical; 10 s, horizontal). (C) Magnified ECoG signal in moving status. (D) Magnified ECoG signal in resting condition. (E) Power spectrum densities of ECoG signal from the motor cortex in moving condition (40–50 s). (F) Power spectrum densities of ECoG signal from the motor cortex in resting condition (90–100 s).

Conclusions

Compared to electroencephalography (EEG), electrocorticography (ECoG) has been favored for a variety of

neuroscience and therapeutic applications because it provides a relatively high spatial resolution while being minimally invasive. However, the surgical procedure over a large area to provide access to the surface of the brain had

limited it from being used to record signals from multi-regions. In this paper, we proposed a new method through which multi-regional recording of ECoG signals can be enabled without extensive exposure of the surface of the brain. With the proposed device, signals from more than one region of interest can be recorded with a minimal surgical procedure. In order to achieve this capability, we minimized the size of the electrodes and implemented the electrode array using thin, long-legged structures. By implementing the electrode array on a polyimide substrate, we provided sufficient flexibility to the electrode array for it to move freely in the epidural space and to conform easily to the curved surface of the brain. By utilizing a miniature neodymium magnet for the accurate positioning of the electrodes to the target area with magnetic force, we minimized the size of the removal on the skull to as small as 1 mm².

We successfully demonstrated that the ECoG electrode array that we fabricated can record ECoG signals from two distant brain regions. In addition, we successfully proved that the electrode array can record multi-regional ECoG signals continuously from freely-moving animals. The signals we recorded from the visual cortex and the motor cortex clearly showed the distinctive signatures of the brain regions, namely the activities induced by the exogenous stimuli and those spontaneously originating from the animal's free behavior, respectively.

With some additional modification of the design or the surgical procedure, the proposed device likely can be used for a wider variety of applications. We demonstrated the capability of the device by recording ECoG signals from two separate regions on the same hemisphere of the brain. With a slightly more sophisticated surgical procedure, ECoG signals may be recorded bilaterally from both hemispheres of the brain by creating a small incision along the sagittal suture and carefully placing the electrodes onto the target regions in both hemispheres. Alternatively, the electrode arrays can be extended to multiple legs and utilized for recording from three or more separate regions of the brain. In this way, the simultaneous monitoring of more than three regions will be achieved, and the investigation of the connectivity of multiple brain regions will be accelerated. The electrode was mechanically strong enough to endure the force for retrieval. If a reversible method for the fixation of the device on the animal head can be developed, the electrode might be reused for experiments in multiple animals as well.

Some ECoG arrays contained a number of perforations at regular intervals of 1 mm or more between their electrodes so that the CSF circulation is not compromised.^{50,51} Considering that the dimensions of the measurement part of the device are as small as 1 × 1 mm and the legs are very narrow (180 μm wide), we believe that the proposed device is free from concern. We did not observe any significant degradation of the recorded signal for 2 weeks. It might be necessary that for long-term chronic experiments that are longer than 2 weeks, CSF circulation must be more carefully

taken into account. It might be inevitable that more perforations are adopted in the future generation of the device and the difference in the tissue reaction becomes confirmed.

While the magnetic positioning of the electrode could be confirmed easily by a visual inspection of the rats, an additional procedure might be required for the application of the proposed ECoG electrode arrays for experiments with different animals. The skull of a rat was thin enough to allow us to see the magnet below the skull, and thus the location of the electrodes could be confirmed easily by a visual inspection under a surgical, bright-field microscope. Although a simple modification of the dimensions of the proposed device would allow it to be used in experiments with a variety of animals, such as rabbits and monkeys, their thicker skulls might prevent the visual inspection of the position of the electrode. Therefore, an additional procedure might be required, such as an inspection with an infrared light source.

We improved the utility of the ECoG by making the experimental procedure even less invasive, and we showed that the new ECoG array facilitates neuroscience experiments in certain animals. The proposed ECoG array may be used in studies to discover the interaction between different cortex regions of the brain during behavior. It also can be used to monitor a subject's status during medical treatment, including clinical procedures. With its advantages, we believe that the proposed device will be used as one of the powerful tools for clinical applications as well as in neuroscientific research.

Author contributions

U. J. and J. L. conceived the study and designed and performed the experiments. U. J. analyzed the data, prepared the figures, and wrote the manuscript. N. C. designed the chronic stimulation experiments. K. K. reviewed and edited the manuscript. H. S. and U. C. provided experimental equipment and technology. I. C. conceived the project and supervised this work as a corresponding author.

Conflicts of interest

There are no conflicts to declare.

Acknowledgements

This research was supported by the Brain Convergence Research Program of the National Research Foundation (NRF) funded by the Korean government (MSIT) (NRF-2019M3E5D2A01063814), the Bio & Medical Technology Development Program of the NRF funded by the Korean government (MSIT) (NRF-2017M3A9B3061319), the Brain Research Program of the NRF funded by the Korean government (MSIT) (NRF-2017M3C7A1028854), and the Korea Institute of Science and Technology (KIST) intramural grant (2E30080, MI). Also, this work was supported by the Institute for Basic Science (IBS-R001-D2).

References

- 1 M. Pievani, N. Filippini, M. P. van den Heuvel, S. F. Cappa and G. B. Frisoni, *Nat. Rev. Neurol.*, 2014, **10**, 620–633.
- 2 M. Straathof, M. R. T. Sinke, T. J. M. Roelofs, E. L. A. Blezer, R. A. Sarabdjitsingh, A. van der Toorn, O. Schmitt, W. M. Otte and R. M. Dijkhuizen, *Sci. Rep.*, 2020, **10**, 56.
- 3 D. Khodagholy, J. N. Gelin, Z. Zhao, M. Yeh, M. Long, J. D. Greenlee, W. Doyle, O. Devinsky and G. Buzsáki, *Sci. Adv.*, 2016, **2**(11), e1601027.
- 4 A. Palmini, A. Gambardella, F. Andermann, F. Dubeau, J. C. da Costa, A. Olivier, D. Tampieri, P. Gloor, F. Quesney and E. Andermann, *et al.*, *Ann. Neurol.*, 1995, **37**, 476–487.
- 5 T. Yang, S. Hakimian and T. H. Schwartz, *Epileptic Disord.*, 2014, **16**, 271–279.
- 6 J. Z. E. Behrens, D. van Roost, A. Hufnagel, C. E. Elger and J. Schramm, *Acta Neurochir.*, 1994, **128**, 84–87.
- 7 H. Toda, T. Suzuki, H. Sawahata, K. Majima, Y. Kamitani and I. Hasegawa, *NeuroImage*, 2011, **54**, 203–212.
- 8 J.-W. Seo, K. Kim, K.-W. Seo, M. K. Kim, S. Jeong, H. Kim, J.-W. Ghim, J. H. Lee, N. Choi, J.-Y. Lee and H. J. Lee, *Adv. Funct. Mater.*, 2020, **30**, 2000896.
- 9 D. Khodagholy, J. N. Gelin, T. Thesen, W. Doyle, O. Devinsky, G. G. Malliaras and G. Buzsáki, *Nat. Neurosci.*, 2015, **18**, 310–315.
- 10 G. Schalk and E. C. Leuthardt, *IEEE Rev. Biomed. Eng.*, 2011, **4**, 140–154.
- 11 D. Khodagholy, J. N. Gelin and G. Buzsáki, *Science*, 2017, **358**, 369–372.
- 12 J. Rivnay, H. Wang, L. Fenno, K. Deisseroth and G. G. Malliaras, *Sci. Adv.*, 2017, **3**, e1601649.
- 13 Z. Shi, F. Zheng, Z. Zhou, M. Li, Z. Fan, H. Ye, S. Zhang, T. Xiao, L. Chen, T. H. Tao, Y. L. Sun and Y. Mao, *Adv. Sci.*, 2019, **6**, 1801617.
- 14 W. S. Konerding, U. P. Friepe, A. Kral and P. Baumhoff, *Sci. Rep.*, 2018, **8**, 3825.
- 15 D. H. Kim, J. Viventi, J. J. Amsden, J. Xiao, L. Vigeland, Y. S. Kim, J. A. Blanco, B. Panilaitis, E. S. Frechette, D. Contreras, D. L. Kaplan, F. G. Omenetto, Y. Huang, K. C. Hwang, M. R. Zakin, B. Litt and J. A. Rogers, *Nat. Mater.*, 2010, **9**, 511–517.
- 16 J. Viventi, D. H. Kim, L. Vigeland, E. S. Frechette, J. A. Blanco, Y. S. Kim, A. E. Avrin, V. R. Tiruvadi, S. W. Hwang, A. C. Vanleer, D. F. Wulsin, K. Davis, C. E. Gelber, L. Palmer, J. Van der Spiegel, J. Wu, J. Xiao, Y. Huang, D. Contreras, J. A. Rogers and B. Litt, *Nat. Neurosci.*, 2011, **14**, 1599–1605.
- 17 B. Rubehn, C. Bosman, R. Oostenveld, P. Fries and T. Stieglitz, *J. Neural Eng.*, 2009, **6**, 036003.
- 18 D. Kuzum, H. Takano, E. Shim, J. C. Reed, H. Juul, A. G. Richardson, J. de Vries, H. Bink, M. A. Dichter, T. H. Lucas, D. A. Coulter, E. Cubukcu and B. Litt, *Nat. Commun.*, 2014, **5**, 5259.
- 19 D. W. Park, S. K. Brodnick, J. P. Ness, F. Atry, L. Krugner-Higby, A. Sandberg, S. Mikael, T. J. Richner, J. Novello, H. Kim, D. H. Baek, J. Bong, S. T. Frye, S. Thongpang, K. I. Swanson, W. Lake, R. Pashaie, J. C. Williams and Z. Ma, *Nat. Protoc.*, 2016, **11**, 2201–2222.
- 20 K. Tybrandt, D. Khodagholy, B. Dielacher, F. Stauffer, A. F. Renz, G. Buzsáki and J. Voros, *Adv. Mater.*, 2018, **30**, e1706520.
- 21 S. Hatashita, J. Koike, T. Sonokawa and S. Ishii, *Stroke*, 1985, **16**, 661–668.
- 22 J. T. Cole, A. Yarnell, W. S. Kean, E. Gold, B. Lewis, M. Ren, D. C. McMullen, D. M. Jacobowitz, H. B. Pollard, J. T. O'Neill, N. E. Grunberg, C. L. Dalgard, J. A. Frank and W. D. Watson, *J. Neurotrauma*, 2011, **28**, 359–369.
- 23 M. M. Koletar, A. Dor, M. E. Brown, J. McLaurin and B. Stefanovic, *Sci. Rep.*, 2019, **9**, 5499.
- 24 A. Vazquez-Guardado, Y. Yang, A. J. Bandodkar and J. A. Rogers, *Nat. Neurosci.*, 2020, **23**, 1522–1536.
- 25 J. Fraden, *Handbook of modern sensors : physics, designs, and applications*, Springer, New York, 4th edn, 2010.
- 26 M. Jeon, J. Cho, Y. K. Kim, D. Jung, E.-S. Yoon, S. Shin and I.-J. Cho, *J. Micromech. Microeng.*, 2014, **24**(2), 025010.
- 27 M. Mathlouthi, *Sucrose : properties and applications*, Springer, 1995.
- 28 V. S. J. M. Camacho, *Rev. Mex. Fis. E*, 2013, **59**(1), 8–17.
- 29 A. D. Tang, A. S. Lowe, A. R. Garrett, R. Woodward, W. Bennett, A. J. Canty, M. I. Garry, M. R. Hinder, J. J. Summers, R. Gersner, A. Rotenberg, G. Thickbroom, J. Walton and J. Rodger, *Front. Neural Circuits*, 2016, **10**(47), DOI: 10.3389/fncir.2016.00047.
- 30 D. Vokoun, M. Beleggia, L. Heller and P. Šittner, *J. Magn. Magn. Mater.*, 2009, **321**, 3758–3763.
- 31 R. Ravaud, G. Lemarquand, S. Babic, V. Lemarquand and C. Akyel, *IEEE Trans. Magn.*, 2010, **46**, 3585–3590.
- 32 S. D. Waldman, *Pain management*, Saunders/Elsevier, Philadelphia, 2007.
- 33 R. J. Low, Y. Gu and D. W. Tank, *Proc. Natl. Acad. Sci. U. S. A.*, 2014, **111**, 18739–18744.
- 34 G. Paxinos and C. Watson, *Paxinos's and Watson's The rat brain in stereotaxic coordinates*, Elsevier/AP, Academic Press is an imprint of Elsevier, Amsterdam, Boston, 7th edn, 2014.
- 35 T. Wanger, K. Takagaki, M. T. Lippert, J. Goldschmidt and F. W. Ohl, *BMC Neurosci.*, 2013, **14**, 78.
- 36 D. T. Bundy, E. Zellmer, C. M. Gaona, M. Sharma, N. Szrama, C. Hacker, Z. V. Freudenburg, A. Daitch, D. W. Moran and E. C. Leuthardt, *J. Neural Eng.*, 2014, **11**, 016006.
- 37 A. G. Siapas and M. A. Wilson, *Neuron*, 1998, **21**, 1123–1128.
- 38 G. Buzsáki, *Brain Res.*, 1986, **398**, 242–252.
- 39 D. P. Nguyen, F. Kloosterman, R. Barbieri, E. N. Brown and M. A. Wilson, *Front. Integr. Neurosci.*, 2009, **3**, 11.
- 40 M. P. Walker and E. M. Robertson, *Curr. Biol.*, 2016, **26**, R239–R241.
- 41 G. Buzsáki, *Rhythms of the brain*, Oxford University Press, Oxford, New York, 2006.
- 42 W. Zhang and M. M. Yartsev, *Cell*, 2019, **178**, 413–428 e422.
- 43 Y. H. Song, J. H. Kim, H. W. Jeong, I. Choi, D. Jeong, K. Kim and S. H. Lee, *Neuron*, 2017, **93**, 940–954 e946.
- 44 S. Gleiss and C. Kayser, *PLoS One*, 2012, **7**, e45677.
- 45 A. Schnitzler and J. Gross, *Nat. Rev. Neurosci.*, 2005, **6**, 285–296.
- 46 I. E. J. Aasebo, M. E. Lepperød, M. Stavrinou, S. Nokkevangen, G. Einevoll, T. Hafting and M. Fyhn, *eNeuro*, 2017, **4**(4), DOI: 10.1523/ENEURO.0059-17.2017.

- 47 A. Y. Tan, Y. Chen, B. Scholl, E. Seidemann and N. J. Priebe, *Nature*, 2014, **509**, 226–229.
- 48 U. Sławińska and S. Kasicki, *Brain Res.*, 1998, **796**, 327–331.
- 49 B. R. Noga, F. J. Sanchez, L. M. Villamil, C. O'Toole, S. Kasicki, M. Olszewski, A. M. Cabaj, H. Majczynski, U. Slawinska and L. M. Jordan, *Front. Neural Circuits*, 2017, **11**, 34.
- 50 T. J. Richner, S. Thongpang, S. K. Brodnick, A. A. Schendel, R. W. Falk, L. A. Krugner-Higby, R. Pashaie and J. C. Williams, *J. Neural Eng.*, 2014, **11**, 016010.
- 51 M. Vomero, M. F. P. Cruz, E. Zucchini, A. Shabanian, E. Delfino, S. Carli, L. Fadiga, D. Ricci and T. Stieglitz, *Conf. Proc. IEEE Eng. Med. Biol. Soc.*, 2018, **2018**, 4464–4467.